A Maximum Likelihood Approach for Image Registration Using Control Point And Intensity

Winston Li and Henry Leung, *Member, IEEE*

***Abstract*—Registration of multidate or multisensor images is an essential process in many image processing applications including remote sensing, medical image analysis, and computer vision. Control point (CP) and intensity are the two basic features used separately for image registration in the literature. In this paper, an exact maximum likelihood (EML) registration method, which combines both CP and intensity, is proposed for image alignment. The EML registration method maximizes the likelihood function based on CP and intensity to estimate the registration parameters, including affine transformation and CP coordinates. The explicit formulas of the Cramer–Rao bound (CRB) are also derived for the proposed EML and conventional image registration algorithms. The performances of these image registration techniques are evaluated with the CRBs.**

***Index Terms*—Affine transformation, control points (CPs), Cramer–Rao bound (CRB), image registration, intensity, maximum likelihood (ML).**

I. Introduction

Registration refers to the process of establishing the geometric transformations between images taken at different times, from different sensors, or from different viewpoints [1]. There are at least three main applications of image registration: remote sensing [2], [3]; medical image analysis [4]; and computer vision [5]–[7]. Registration is an important preprocessing step for fusion of remote-sensing images. In medical imaging, image registration is a vital component for a large number of applications such as clinical diagnostic, radiotherapy treatment, and surgery. In computer vision, image registration is required for motion tracking, object recognition, and shape reconstruction.

Many image registration algorithms have been proposed based on different image features and criteria. Intensity and control points (CPs) are two basic features used for image registrations in the literature. While intensity is the gray value of a pixel, CPs are pixel points, such as corners, road intersections, points of locally maximum curvature, and centers of gravity of close-boundary regions in an image [8]–[10]. Most CP-based methods use a least-squares (LS) criterion to estimate the registration parameters [11], [12], and the intensity approach might use the normalized cross-correlation [13], LS [14], and maximum likelihood (ML) criteria [15], [16]. The CP and intensity approaches have their own advantages and disadvantages. The CP approach has a low computation complexity, but its registration accuracy might be poor. The intensity approach has a more accurate registration, but it cannot be applied to some applications such as image-to-map registration because the intensity information is not available in the reference map. In addition, the computation load of the intensity approach is fairly high. Recently, combination of different registration methods has becoming a promising approach to improve the performance of image registration. The landmark registration and intensity registration are used iteratively to align nonrigid magnetic resonance images [17]. A hybrid registration method is proposed in [18] that takes advantages of both optical flow-based photometric registration and landmark-based registration, but due to the lack of a rigorous measure for the image registrations, it is difficult to assess the performance of an image registration technique.

In this paper, an exact maximum likelihood (EML) [19] image registration method is proposed. It uses both CP and intensity features in a unified framework to compute the registration parameters. A single cost function is defined based on both features. When either information is not available or has a poor measured quality, the EML method can still be used to align images. When there is no CP, the EML method can be shown to be equivalent to the intensity-based ML registration approach. When the intensity information is not available, the EML method becomes a ML approach for the CP-based registration. We also show here that when the CP measurement noise level is high, the ML approach for CP-based registration is superior to the conventional CP-based LS approach.

To evaluate the performance of an image registration algorithm, we propose to use the Cramer–Rao (CRB) to assess the theoretical limit of image registration. CRB is widely used in statistical signal processing to determine the fundamental limit on estimation accuracy [20]–[22]. Although image registration is usually considered as a parameter estimation problem, to the best of our knowledge, such a theoretical limit for image registration has not yet been developed. In this paper, we derive the CRBs for the conventional CP and intensity approaches as well as the proposed EML approach. Based on these bounds, we can evaluate the effectiveness of using CP and intensity for image registration, and the efficiency of the estimation techniques in achieving the registration limit.

This paper is organized as follows. Section II introduces our proposed unified CP and intensity-based EML image registra-

Manuscript received July 21, 2003; revised January 26, 2004. The associate editor coordinating the review of this manuscript and approving it for publication was Prof. Bruno Carpentieri.

The authors are with the Department of Electrical and Computer Engineering, University of Calgary, Calgary, AB T2N 1N4, Canada (e-mail: winston_li66@yahoo.com; leungh@enel.ucalgary.ca).

Digital Object Identifier 10.1109/TIP.2004.828435

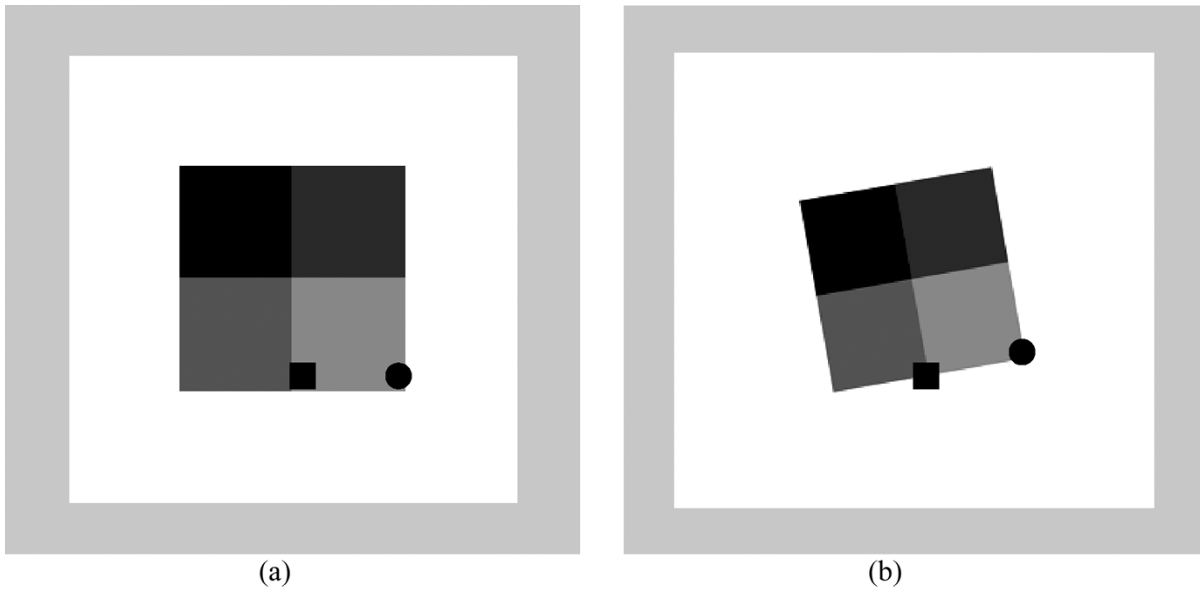

Fig. 1. EML image registration method uses both CP and intensity. (a) Reference image. (b) Distorted image. The first corresponding CPs are represented by the circles and the second corresponding CPs are represented by the squares.

tion model. Section III presents the EML algorithm that estimates the registration parameters of the unified model. The CRBs of the EML method and the conventional CP and intensity approaches are derived in Section IV. Experimental results are presented in Section V to evaluate the performance of the proposed EML and to compare with the conventional image registration methods. Conclusions are given in Section VI.

II. Image Registration Model

To align a distorted image through some affine transformation to a reference image as shown in Fig. 1, either CP or the intensity information is usually used in the conventional image registration approaches. Suppose that the number of CPs is N_1, the number of overlapped pixels between the reference and distorted images is N_2, and the measurement noises on the N_1 CPs and on the N_2 overlapped pixels are independent white Gaussian, we can then formulate the image registration as a ML estimation problem based on both CP and intensity. The measurement models of the CPs and intensity are first introduced here. Based on these measurement models, we develop a unified model for image registration.

A. CP Measurement Model

Let $\boldsymbol{X}_1(k) = [x_1(k), y_1(k)]^T$ and $\boldsymbol{X}_0(k) = [x_0(k), y_0(k)]^T$ denote the true coordinates of the kth corresponding CPs in the reference and distorted images, respectively, $k = 1, 2, \ldots, N_1$ where N_1 is the total number of CPs. These CPs can be linked by an affine transformation given by

$$\boldsymbol{X}_1(k) = \boldsymbol{t} + \boldsymbol{R}\boldsymbol{X}_0(k),\ k = 1,\ 2,\ \ldots,\ N_1 \tag{1}$$

where $\boldsymbol{t} = [tx,\ ty]^T$ represents the x- and y-axis translations, $\boldsymbol{R}$ is the affine transformation matrix between the reference and distorted images and is given by

$$\boldsymbol{R} = \begin{pmatrix} 1 + r_{11} & r_{12} \\ r_{21} & 1 + r_{22} \end{pmatrix} \tag{2}$$

where the diagonal elements of $\boldsymbol{R}$ are defined as $(1 + r_{11})$ and $(1 + r_{22})$ so as to simplify the derivation of the recursive optimization of the EML image registration method. The four elements of $\boldsymbol{R}$ cover any combination of rotation, skewing, shearing, and scaling between the reference and distorted images.

Let $\boldsymbol{X}_A(k) = [x_A(k),\ \ y_A(k)]^T$ and $\boldsymbol{X}_B(k) = [x_B(k),\ \ y_B(k)]^T$ denote the measured coordinates of the corresponding CPs in the reference and distorted images, respectively, $k = 1, 2, \ldots, N_1$. The CP measurement model can be expressed as

$$\begin{aligned} x_A(k) &= x_0(k) + n_1(k) \\ y_A(k) &= y_0(k) + n_2(k) \\ x_B(k) &= (1 + r_{11})x_0(k) + r_{12}y_0(k) + tx + n_3(k) \\ y_B(k) &= r_{21}x_0(k) + (1 + r_{22})y_0(k) + ty + n_4(k) \end{aligned} \tag{3}$$

where n_i and $i = 1, 2, 3, 4$ are white Gaussian noise with zero mean and variance δ_1^2.

Equation (3) can be written in matrix form as

$$\boldsymbol{x}(k) = \boldsymbol{A}(k)\boldsymbol{\eta} + \boldsymbol{b}(k) + \boldsymbol{n}(k) \tag{4}$$

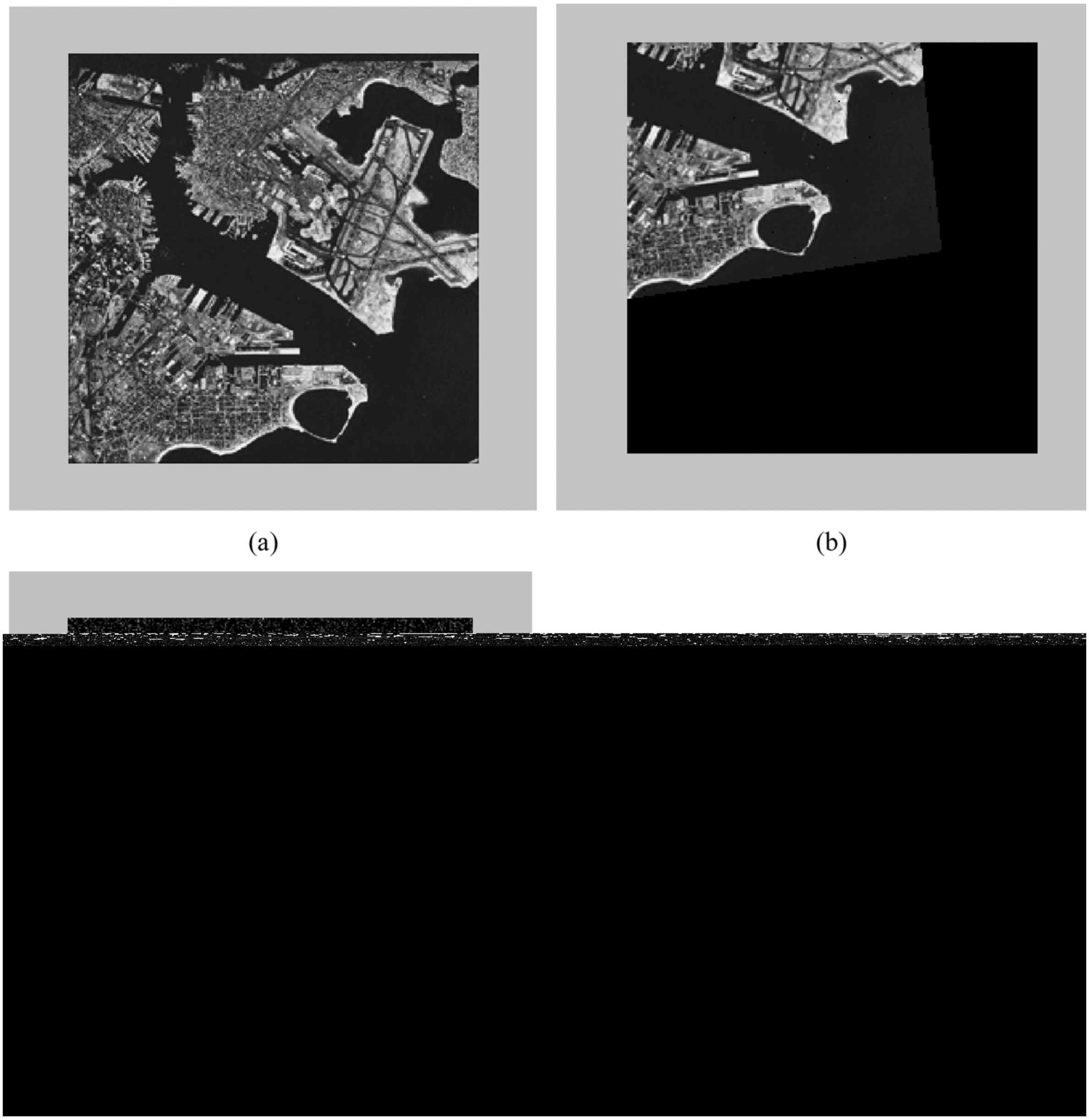

Fig. 2. First remote-sensing image example. (a) Reference image. (b) and (c) Two distorted images after some affine transformations.

where

$$
\begin{aligned}
\boldsymbol{x}(k) &= [(\boldsymbol{X}_A(k))^T,\ (\boldsymbol{X}_B(k))^T]^T \\
\boldsymbol{b}(k) &= [(\boldsymbol{X}_0(k))^T,\ (\boldsymbol{X}_0(k))^T]^T \\
\boldsymbol{n}(k) &= [n_1(k), n_2(k), n_3(k), n_4(k)]^T \\
\boldsymbol{\eta} &= [\eta_1, \eta_2, \eta_3, \eta_4, \eta_5, \eta_6]^T = [r_{11}, r_{12}, r_{21}, r_{22}, tx, ty]^T \\
\boldsymbol{A}(k) &= \begin{pmatrix} 0 & 0 & 0 & 0 & 0 & 0 \\ 0 & 0 & 0 & 0 & 0 & 0 \\ x_0(k) & y_0(k) & 0 & 0 & 1 & 0 \\ 0 & 0 & x_0(k) & y_0(k) & 0 & 1 \end{pmatrix}.
\end{aligned}
$$

$\boldsymbol{x}(k), \boldsymbol{n}(k)$, and $\boldsymbol{\eta}$ represent the vectors for measurements, noise, and registration parameters, respectively. The covariance matrix of $\boldsymbol{n}(k)$ is equal to $\delta_1^2 \boldsymbol{I}$, where $\boldsymbol{I}$ is the identity matrix.

B. Intensity Measurement Model

Assume that the size of the reference image is $M_1 \times M_2$. Let Ω denote the overlapping region of the reference and distorted images, and there are N_2 pixels in Ω. Given the coordinate $\boldsymbol{u}_0(i,\ j) = [u_0(i),\ v_0(j)]^T$ of a pixel in the reference image, the coordinate $\boldsymbol{u}_1(i,\ j) = [u_1(i),\ v_1(j)]^T$ of the corresponding pixel in the distorted image can be related by

$$\boldsymbol{u}_1(i,\ j) = \boldsymbol{t} + \boldsymbol{R}\boldsymbol{u}_0(i,\ j) \tag{5}$$

where $i = 1, 2, \ldots, M_1,\ j = 1, 2, \ldots, M_2$, and $\boldsymbol{t}$ and $\boldsymbol{R}$ are the affine transformation parameters to be estimated. Suppose that the true gray values of pixels $\boldsymbol{u}_1(i, j)$ and $\boldsymbol{u}_0(i,\ \ j)$ are

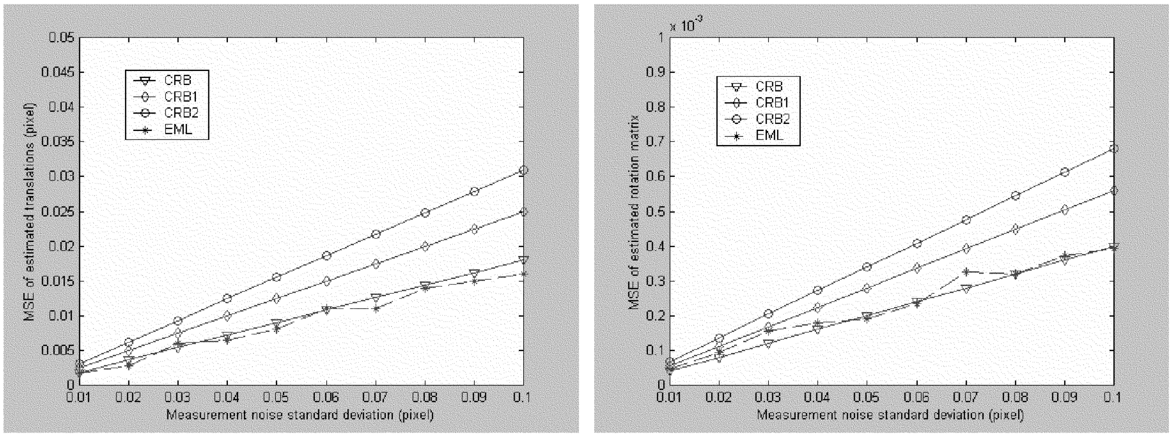

(a) (b)

Fig. 3. Evaluation of the registration MSE of the EML algorithm versus the measurement noise deviation for the images in Fig. 2(a) and (b). (a) Translation MSE. (b) MSE for the affine matrix. $N_1 = 200, N_2 = 2500$, and δ_1 changes from 0.01 to 0.1 subpixel and δ_2 changes from 10 to 100.

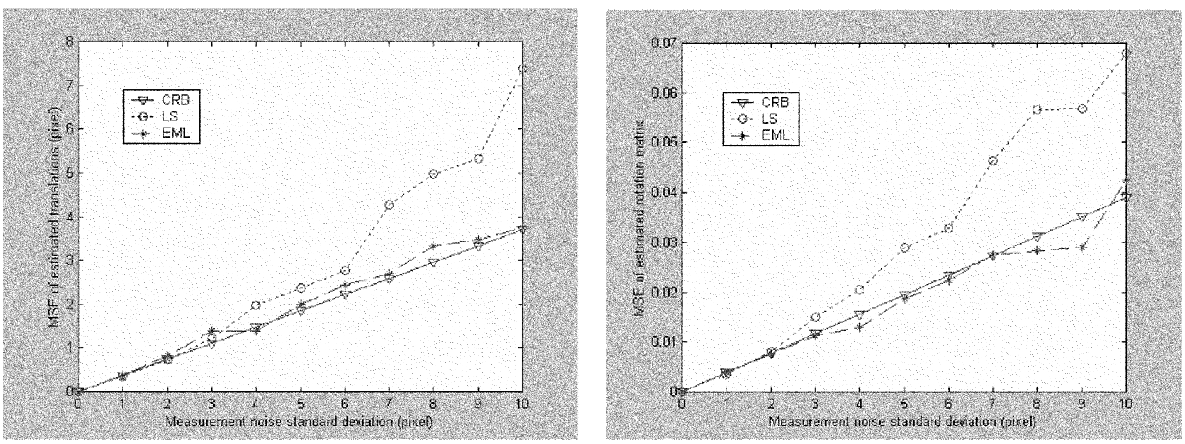

(a) (b)

Fig. 4. Comparison of the CRBs and MSEs of the estimated translations and affine matrix obtained by the EML image registration method and the conventional CP-based LS method. The MSE is plotted versus the CP measurement noise deviation for the images in Fig. 2(a) and (c). (a) Translation MSE. (b) MSE for the affine matrix. $N_1 = 100, N_2 = 0$, and δ_1 changes from 0 to 10 pixels. $CRB[\boldsymbol{\eta}] = CRB_1[\boldsymbol{\eta}]$.

$f_1(\boldsymbol{u}_1(i,\ j))$ and $f_0(\boldsymbol{u}_0(i,\ j))$, correspondingly, the measured gray value of the pixel $\boldsymbol{u}_1(i,\ j)$ can be expressed as

$$f_A(\boldsymbol{u}_1(i,\ j)) = f_1(\boldsymbol{u}_1(i,\ j)) + n_5(i,\ j) \tag{6}$$

where $n_5(i,j)$ is a white Gaussian noise process with zero mean and variance δ_2^2.

C. EML Image Registration Model

Based on the CP and intensity measurement models in (4) and (6), we propose the following unified registration model for the EML approach. Assume that the measurements noises of CPs and intensity are independent white Gaussian, then the conditional density function for the N_1 CP measurements $\boldsymbol{x}(k), k = 1, 2, \ldots, N_1$, and for the N_2 intensity measurements $f_A(\boldsymbol{u}_1(i,j)), (i,j) \in \Omega$, can be written as [23]

$$L = \frac{1}{\left(\sqrt{2\pi}\right)^{N_1+N_2} \delta_1^{N_1} \delta_2^{N_2}} L_1 L_2 \tag{7}$$

where

$$L_1 = \exp\left\{-\frac{1}{2\delta_1^2}\Gamma_1\right\}, \quad L_2 = \exp\left\{-\frac{1}{2\delta_2^2}\Gamma_2\right\}$$
$$\Gamma_1 = \sum_{k=1}^{N_1} \{\boldsymbol{x}(k) - \boldsymbol{A}(k)\boldsymbol{\eta} - \boldsymbol{b}(k)\}^T \{\boldsymbol{x}(k) - \boldsymbol{A}(k)\boldsymbol{\eta} - \boldsymbol{b}(k)\}$$
$$\Gamma_2 = \sum_{(i,j)\in\Omega}^{N_2} \{f_A(\boldsymbol{u}_1(i,j)) - f_0(\boldsymbol{u}_0(i,j))\}^2. \tag{8}$$

For the reference image, $u_0(i) = i, v_0(j) = j$, and $(i,\ j) \in \Omega$, i.e., (i,j) is the coordinate of an overlapped pixel between the reference and distorted images. L_1 is determined by the CP measurements $\boldsymbol{x}(k)$ and $k = 1, 2, \ldots, N_1$. The unknown parameters in L_1 include the affine transformation $\boldsymbol{\eta}$, the CP coordinates $\boldsymbol{\xi}(k) = [x_0(k),\ y_0(k)]^T$, $k = 1, 2, \ldots, N_1$, and the CP measurement noise variance δ_1^2. L_2 is determined by the intensity measurements. The unknown parameters in L_2 include the affine transformation $\boldsymbol{\eta}$ and the intensity measurement noise variance δ_2^2. These unknown parameters will be estimated by

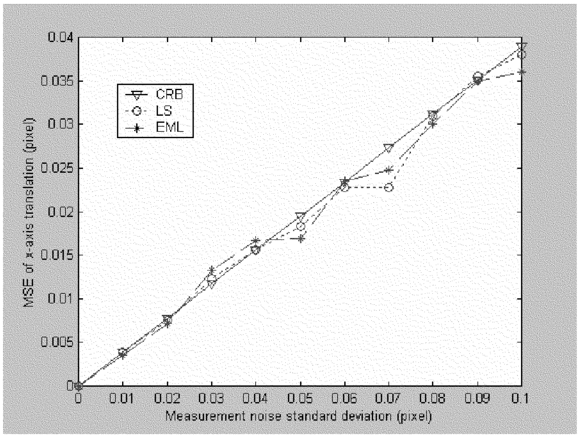

(a)

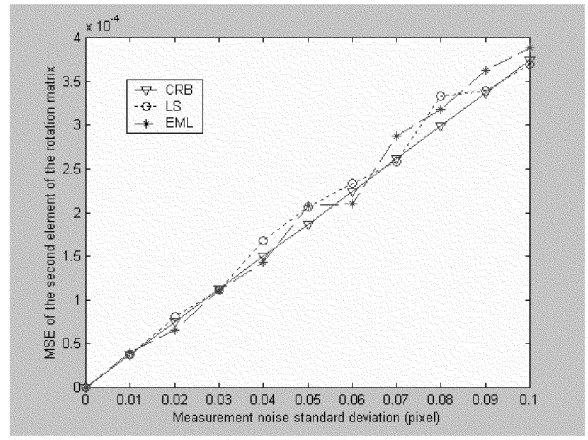

(b)

Fig. 5. Comparison of the CRBs and MSEs of the estimated translations and affine matrix obtained by the EML image registration method and the conventional CP-based LS method. The MSE is plotted versus the CP measurement noise deviation in the subpixel level. (a)Translation MSE. (b) MSE for the affine matrix. $N_1 = 100$, $N_2 = 0$, and δ_1 changes from 0.0 to 0.10 subpixel. $CRB[\boldsymbol{\eta}] = CRB_1[\boldsymbol{\eta}]$.

maximizing the likelihood function L based on the N_1 CP measurements and N_2 intensity measurements.

When there is no CP, $N_1 = 0$, (7) becomes the likelihood function of the conventional intensity-based ML registration method [15], [16]

$$L = \frac{1}{\left(\sqrt{2\pi}\right)^{N_2} \delta_2^{N_2}} L_2. \tag{9}$$

When the intensity information is not available, $N_2 = 0$, (7) can be expressed as

$$L = \frac{1}{\left(\sqrt{2\pi}\right)^{N_1} \delta_1^{N_1}} L_1 = \frac{1}{\left(\sqrt{2\pi}\right)^{N_1} \delta_1^{N_1}} \exp\left\{-\frac{1}{2\delta_1^2}\Gamma_1\right\}. \tag{10}$$

The objective function of the conventional CP-based LS method can also be linked to the likelihood function in (10) by [2]

$$L_{LS} = \frac{1}{N_1}\Gamma_1. \tag{11}$$

III. EML Image Registration Algorithm

Based on the EML image registration model in (7), an iterative optimization technique can be applied to maximize the likelihood function. The unknown parameters include the affine transformation $\boldsymbol{\eta}$, the CP coordinates $\boldsymbol{\xi}(k)$, $k = 1, 2, \ldots, N_1$, CP measurement noise variance δ_1^2, and intensity measurement noise variance δ_2^2. We first derive the estimation formulas for δ_1^2 and δ_2^2. The EML algorithm is then used to estimate the coordinates $\boldsymbol{\xi}(k)$ and the registration parameter $\boldsymbol{\eta}$ recursively.

Without loss of generality, we ignore the constant term in deriving the optimization process, and the corresponding negative log likelihood function of (7) becomes

$$\Lambda = -\log L = \Lambda_1 + \Lambda_2 \tag{12}$$

where

$$\begin{aligned} \Lambda_1 &= N_1 \ln(\delta_1) + \frac{1}{2\delta_1^2}\Gamma_1 \\ \Lambda_2 &= N_2 \ln(\delta_2) + \frac{1}{2\delta_2^2}\Gamma_2. \end{aligned} \tag{13}$$

Note that Λ is a function of δ_1^2, δ_2^2, $\boldsymbol{\eta}$, and $\boldsymbol{\xi}(k)$. If we set δ_2^2, $\boldsymbol{\eta}$, and $\boldsymbol{\xi}(k)$ equal to their estimates, i.e., $\delta_2^2 = \hat{\delta}_2^2$, $\boldsymbol{\eta} = \hat{\boldsymbol{\eta}}$, $\boldsymbol{\xi}(k) = \hat{\boldsymbol{\xi}}(k) = [\hat{x}_0(k),\ \hat{y}_0(k)]^T$, $k = 1, 2, \ldots, N_1$, and minimize Λ with respect to δ_1, then δ_1^2 can be estimated by

$$\begin{aligned} \hat{\delta}_1^2 = \frac{1}{N_1}\sum_{k=1}^{N_1} &(\boldsymbol{x}(k) - \hat{\boldsymbol{A}}(k)\hat{\boldsymbol{\eta}} \\ &- \hat{\boldsymbol{b}}(k))^T(\boldsymbol{x}(k) - \hat{\boldsymbol{A}}(k)\hat{\boldsymbol{\eta}} - \hat{\boldsymbol{b}}(k)). \end{aligned} \tag{14}$$

Similarly, by setting δ_1^2, $\boldsymbol{\eta}$, and $\boldsymbol{\xi}(k)$ equal to their estimates, i.e., $\delta_1^2 = \hat{\delta}_1^2$, $\boldsymbol{\eta} = \hat{\boldsymbol{\eta}}$, $\boldsymbol{\xi}(k) = \hat{\boldsymbol{\xi}}(k)$, and minimizing Λ with respect to δ_2, the estimate of δ_2^2 is given by

$$\hat{\delta}_2^2 = \frac{1}{N_2}\sum_{(i,j)\in\Omega}^{N_2} \left\{f_A(\hat{\boldsymbol{t}} + \hat{\boldsymbol{R}}\boldsymbol{u}_0(i,\ j)) - f_0(\boldsymbol{u}_0(i,\ j))\right\}^2. \tag{15}$$

Substituting $\hat{\delta}_1^2$ and $\hat{\delta}_2^2$ back into (12), we can solve for $\boldsymbol{\xi}(k)$ and $\boldsymbol{\eta}$. That is

$$[\hat{\boldsymbol{\xi}}(k), \hat{\boldsymbol{\eta}}] = \arg\min_{\boldsymbol{\xi}(k),\boldsymbol{\eta}} \Lambda \Big|_{\delta_1=\hat{\delta}_1,\ \delta_2=\hat{\delta}_2} \tag{16}$$

Because an analytical solution for $\boldsymbol{\xi}(k)$ and $\boldsymbol{\eta}$ is hard to derive, an iterative optimization method is used here. We divide the EML image registration algorithm into two steps to estimate $\boldsymbol{\xi}(k)$ and $\boldsymbol{\eta}$. First, $\boldsymbol{\xi}(k)$ is estimated while $\boldsymbol{\eta}$ is held fixed at its estimate $\hat{\boldsymbol{\eta}}$. Then, $\boldsymbol{\eta}$ is updated by using the current estimate of CP coordinates. We will keep iterating these steps until the final convergence is achieved.

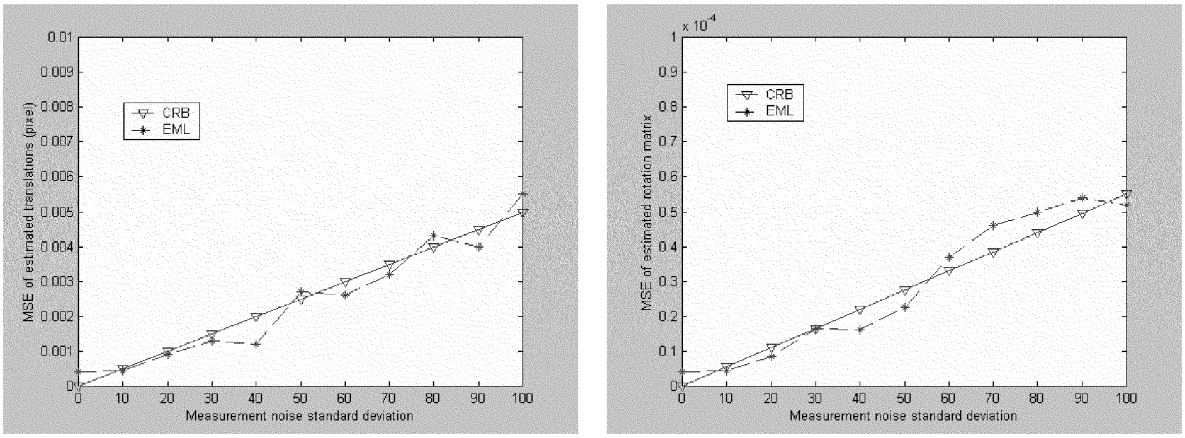

(a) (b)

Fig. 6. Comparison of the CRBs and MSEs of the estimated translations and affine matrix obtained by the intensity-based EML image registration method. The MSE is plotted versus the intensity measurement noise deviation for the images in Fig. 2(a) and (c). (a) Translation MSE. (b) MSE for the affine matrix. $N_1 = 0, N_2 = 10\,000$, and δ_2 changes from 0.0 to 100. $CRB[\boldsymbol{\eta}] = CRB_2[\boldsymbol{\eta}]$.

A. Estimating $\boldsymbol{\xi}(k)$ With $\boldsymbol{\eta}$ Being Held Fixed

By setting the affine transformation parameter $\boldsymbol{\eta}$ as its estimate $\hat{\boldsymbol{\eta}} = [\hat{r}_{11}, \hat{r}_{12}, \hat{r}_{21}, \hat{r}_{22}, \hat{t}x, \hat{t}y]^T$, the CP coordinate $\boldsymbol{\xi}(k)$ can be estimated as

$$\hat{\boldsymbol{\xi}}(k) = \arg\min_{\boldsymbol{\xi}(k)} \Lambda \Big|_{\boldsymbol{\eta}=\hat{\boldsymbol{\eta}}}, k = 1, 2, \ldots, N_1. \tag{17}$$

Since $\hat{\boldsymbol{\xi}}(k)$ is a minimum of Λ given $\hat{\boldsymbol{\eta}}$, the first derivatives of Λ should be zero, i.e., $\partial\Lambda/\partial\boldsymbol{\xi}(k)\Big|_{\boldsymbol{\xi}(k)=\hat{\boldsymbol{\xi}}(k)} = 0$. That is

$$\begin{aligned}\frac{\partial\Lambda}{\partial\boldsymbol{\xi}(k)} &= -\frac{1}{\hat{\delta}_1^2}(\boldsymbol{x}(k) - \boldsymbol{A}(k)\hat{\boldsymbol{\eta}} - \boldsymbol{b}(k))^T \frac{\partial(\boldsymbol{x}(k) - \boldsymbol{A}(k)\hat{\boldsymbol{\eta}} - \boldsymbol{b}(k))}{\partial\boldsymbol{\xi}(k)} \\ &= -\frac{1}{\hat{\delta}_1^2}(\boldsymbol{x}(k) - \boldsymbol{A}(k)\hat{\boldsymbol{\eta}} - \hat{\boldsymbol{b}}(k))^T \left(-\frac{\partial\boldsymbol{A}(k)}{\partial\boldsymbol{\xi}(k)} - \frac{\partial b(k)}{\partial\boldsymbol{\xi}(k)}\right) \\ &= \mathbf{0}.\end{aligned} \tag{18}$$

From (18), we have

$$\boldsymbol{C}\boldsymbol{\xi}(k) = \boldsymbol{D}(k) \tag{19}$$

where

$$\begin{aligned}\boldsymbol{C} &= \boldsymbol{I}_2 + \hat{\boldsymbol{R}}^T\hat{\boldsymbol{R}}, \ \boldsymbol{I}_2 \text{ is a } 2\times 2 \text{ identity matrix} \\ \boldsymbol{D}(k) &= \boldsymbol{X}_A(k) + \hat{\boldsymbol{R}}^T\left(\boldsymbol{X}_B(k) - \hat{\boldsymbol{t}}\right).\end{aligned} \tag{20}$$

By solving (19), we can obtain an optimal estimate of $\boldsymbol{\xi}(k)$ for $k = 1, 2, \ldots, N_1$

$$\hat{\boldsymbol{\xi}}(k) = \boldsymbol{C}^{-1}\boldsymbol{D}(k). \tag{21}$$

B. Estimating $\boldsymbol{\eta}$ With $\boldsymbol{\xi}(k)$ Being Held Fixed

Based on the estimate $\hat{\boldsymbol{\xi}}(k) = [\hat{x}_0(k),\ \hat{y}_0(k)]^T$ obtained in the previous step, we can get an update of the estimate of $\boldsymbol{\eta}$ by a method similar to the Marquardt–Levenberg strategy in [14]. That is

$$\hat{\boldsymbol{\eta}}^{(t+1)} = \hat{\boldsymbol{\eta}}^{(t)} - \alpha\left(\nabla^2\Lambda + \lambda\boldsymbol{I}\right)^{-1}\nabla\Lambda \tag{22}$$

where α and λ are constants, and $\boldsymbol{I}$ is the identity matrix. When $\alpha = 1$, (22) becomes the standard Marquardt–Levenberg strategy in [14]. When $\lambda = 0$, it becomes the Newton optimization method in [19].

The derivative of Λ with respect to $\boldsymbol{\eta}$ can be derived from (12). That is

$$\nabla\Lambda = \frac{\partial\Lambda}{\partial\boldsymbol{\eta}} = \frac{\partial\Lambda_1}{\partial\boldsymbol{\eta}} + \frac{\partial\Lambda_2}{\partial\boldsymbol{\eta}} \tag{23}$$

where

$$\begin{aligned}\frac{\partial\Lambda_1}{\partial\boldsymbol{\eta}} &= -\frac{1}{\hat{\delta}_1^2}\sum_{k=1}^{N_1}\hat{\boldsymbol{A}}^T(k)[\boldsymbol{x}(k) - \hat{\boldsymbol{A}}(k)\boldsymbol{\eta}_1 - \hat{\boldsymbol{b}}(k)] \\ \frac{\partial\Lambda_2}{\partial\eta_k} &= \frac{1}{\hat{\delta}_2^2}\sum_{(i,j)\in\Omega}^{N_2}[f_A(\boldsymbol{u}_1(i,j)) - f_0(\boldsymbol{u}_0(i,j))]\frac{\partial f_A(\boldsymbol{u}_1(i,j))}{\partial\eta_k}.\end{aligned} \tag{24}$$

When intensity is missing, the estimate $\hat{\boldsymbol{\eta}}^{(t+1)}$ can be obtained directly by solving (24), and is given by

$$\hat{\boldsymbol{\eta}}^{(t+1)} = \left\{\sum_{k=1}^{N_1}\hat{\boldsymbol{A}}^T(k)\hat{\boldsymbol{A}}(k)\right\}^{-1}\sum_{k=1}^{N_1}\hat{\boldsymbol{A}}^T(k)[\boldsymbol{x}(k) - \hat{\boldsymbol{b}}(k)]. \tag{25}$$

The Hessian matrix $\nabla^2\Lambda$ are determined by

$$\nabla^2\Lambda = \nabla^2\Lambda_1 + \nabla^2\Lambda_2 \tag{26}$$

where the elements of $\nabla^2\Lambda_1$ and $\nabla^2\Lambda_2$ are given by

$$\begin{aligned}\frac{\partial^2\Lambda_1}{\partial\eta_k\partial\eta_j} &= \frac{1}{\hat{\delta}_1^2}\sum_{k=1}^{N_1}\hat{\boldsymbol{A}}^T(k)\hat{\boldsymbol{A}}(k) \\ \frac{\partial^2\Lambda_2}{\partial\eta_k\partial\eta_l} &= \frac{1}{\hat{\delta}_2^2}\sum_{(i,j)\in\Omega}^{N_2}\frac{\partial f_A(\boldsymbol{u}_1(i,j))}{\partial\eta_k}\frac{\partial f_A(\boldsymbol{u}_1(i,j))}{\partial\eta_l}.\end{aligned} \tag{27}$$

$\partial f_A(\boldsymbol{u}_1(i,j))/\partial\eta_k$ can be computed by using the similar method. For instance

$$\frac{\partial f_A(\boldsymbol{u}_1(i,j))}{\partial tx} = \frac{\partial f_A(\boldsymbol{u}_1(i,j))}{\partial u_1(i)}\frac{\partial u_1(i)}{\partial tx}. \tag{28}$$

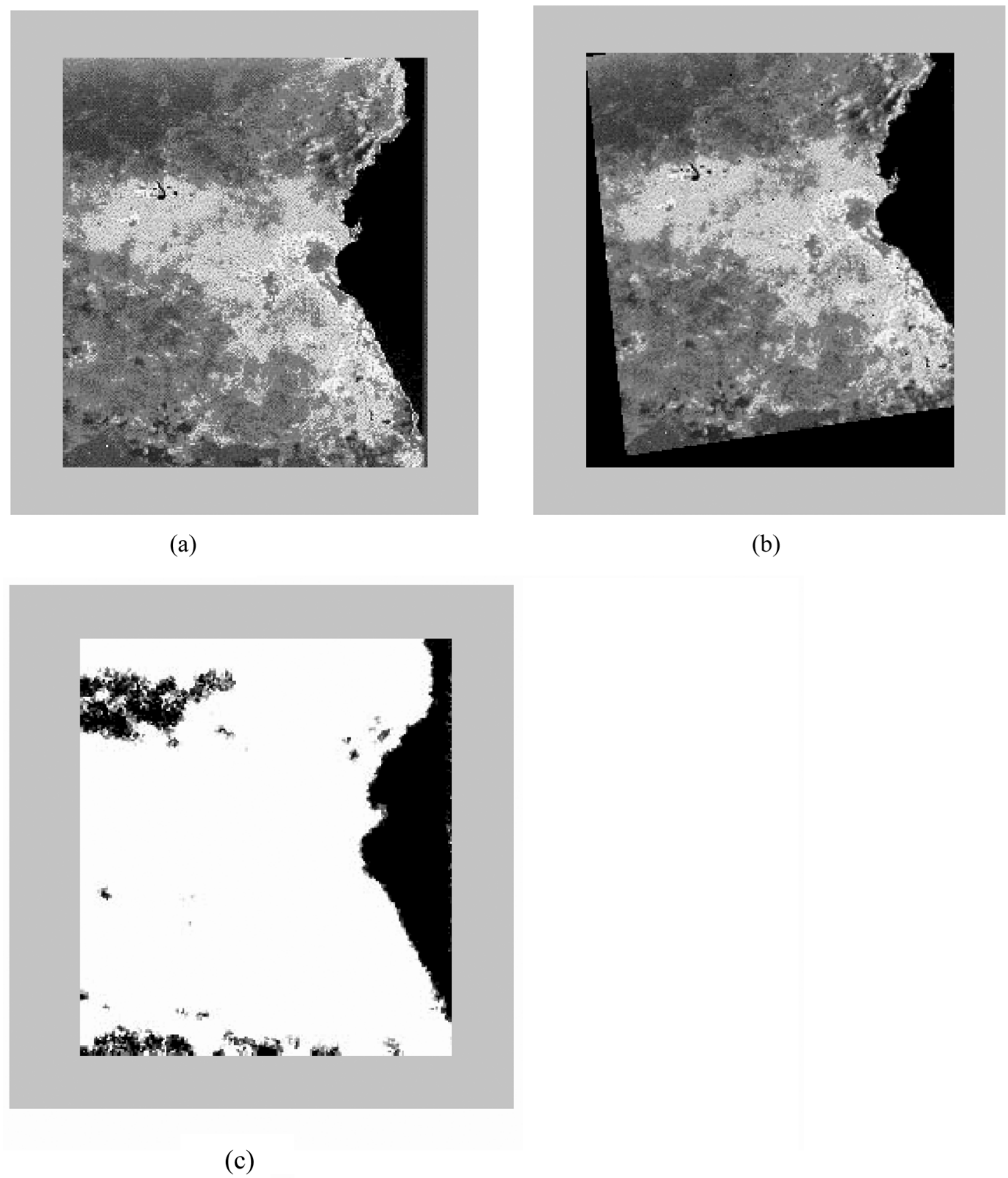

Fig. 7. Second remote-sensing image example. (a) Reference image. (b) Distorted image with similar intensity. (c) Distorted image in which intensity variation is large.

From (5), we have $\partial u_1(i)/\partial tx = 1$. To compute $\partial f_A(\mathbf{u}_1(i,\ j))/\partial u_1(i)$, a cubic convolution interpolation with the following kernel is used [24]

$$z(s) = \begin{cases} \frac{3}{2}\left|s\right|^3 - \frac{5}{2}\left|s\right|^2 + 1, & 0 < |s| < 1 \\ -\frac{1}{2}\left|s\right|^3 + \frac{5}{2}\left|s\right|^2 - 4\left|s\right| + 2, & 1 < |s| < 2 \\ 0, & 2 < |s| \end{cases} . \tag{29}$$

Suppose that $\boldsymbol{u}_1(i,\ j)$ is a pixel point located in the rectangular subdivision $[U(i), U(i+1)] \times [V(j), V(j+1)]$ in image f_A where $U(i)$ and $V(j)$ are integers, i.e., $U(i) \leq u_1(i) \leq U(i+1)$, and $V(j) \leq v_1(j) \leq V(j+1)$. $f_A(\boldsymbol{u}_1(i,\ j))$ can be obtained by using the above cubic convolution interpolation kernel

$$f_A(\boldsymbol{u}_1(i,j)) = \sum_{l=-1}^{2}\sum_{m=-1}^{2} c_{i+l,j+m}\, z\left(\frac{u_1(i) - U(i+l)}{h_x}\right) z \times \left(\frac{v_1(j) - V(j+m)}{h_y}\right) \tag{30}$$

where h_x and h_y are the sampling increments in the x and y axis, respectively, and $c_{ij} = f_A(U(i), V(j))$ is the gray value.

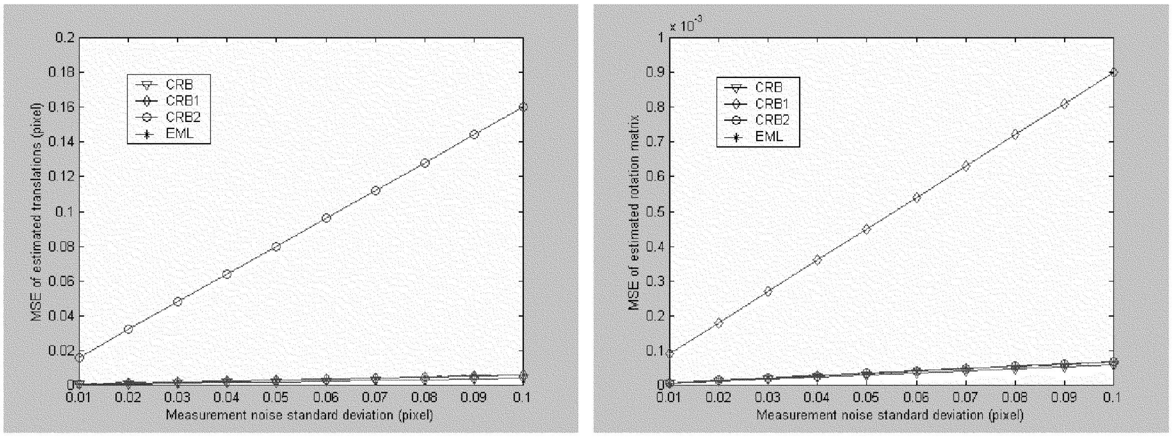

(a) (b)

Fig. 8. Evaluation of the registration MSE of the EML algorithm versus the measurement noise deviation for the images shown in Fig. 7(a) and (b). (a) Translation MSE. (b) MSE for the affine matrix. $N_1 = 100, N_2 = 10\,000$, and δ_1 changes from 0.01 to 0.1 subpixel, and δ_2 changes from 10 to 100.

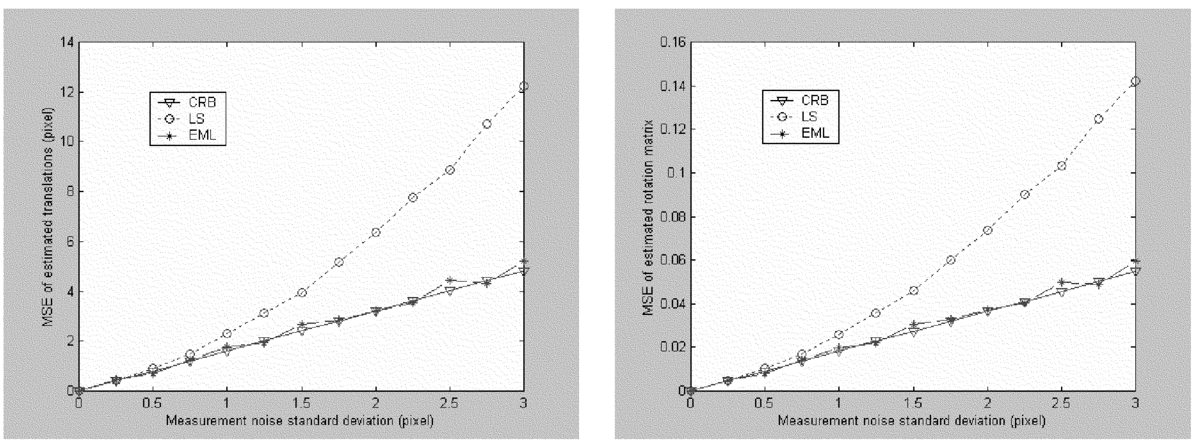

(a) (b)

Fig. 9. Comparison of the CRBs and MSEs of estimated translations and affine matrix obtained by the EML image registration method and the conventional CP-based LS method. The MSE is plotted versus the CP measurement noise deviation for the images in Fig. 7(a) and (c). (a)Translation MSE. (b) MSE for the affine matrix. $N_1 = 100, N_2 = 0$, and δ_1 changes from 0 to 3.0 pixels. $CRB[\boldsymbol{\eta}] = CRB_1[\boldsymbol{\eta}]$.

$\partial f_A(\boldsymbol{u}_1(i,\, j))/\partial u_1(i)$ and $\partial f_A(\boldsymbol{u}_1(i,\, j))/\partial v_1(j)$ can then be derived from (30).

The procedures of the EML image registration algorithm are summarized in the following steps.

Step 1) Set an error threshold ε and the maximum iteration time $t_{\max}$.
Step 2) Initialize $\boldsymbol{\eta}^{(0)}$, $\delta_1^{(0)}$, $\delta_2^{(0)}$ and start the iteration.
Step 3) Estimate the CP coordinate $\boldsymbol{\xi}^{(t)}(k)$ using (21) for $k = 1, 2, \ldots, N_1$.
Step 4) Estimate $\boldsymbol{\eta}^{(t)}$ using intensity and estimated CP coordinates in the Step 3).
a) Estimate $\partial f_A(\boldsymbol{u}_1(i,\, j))/\partial u_1(i)$ and $\partial f_A(\boldsymbol{u}_1(i,\, j))/\partial v_1(j)$ using (30).
b) Estimate $\nabla\Lambda$ and $\nabla^2\Lambda$ by (23) and (26).
c) When only CPs are available, estimate $\boldsymbol{\eta}^{(t)}$ by (25).
Step 5) Estimate $\delta_1^{(t)}$ and $\delta_2^{(t)}$ by using $\boldsymbol{\xi}^{(t)}(k)$, $\boldsymbol{\eta}^{(t)}$, and (14) and (15). λ is updated according to [14, Appendix]. α is decreased after a few iterations.
Step 6) If $t = t_{\max}$, or $\left\|\hat{\boldsymbol{\eta}}^{(t)} - \hat{\boldsymbol{\eta}}^{(t-1)}\right\| < \varepsilon$, go to Step 7); else, go to Step 3).
Step 7) Stop.

IV. CRB of the EML Image Registation Method

CRB is a performance bound that measures the accuracy limit of a parameter estimate. By observing the differences between the CRB and the mean square error (MSE) of the estimates, we can evaluate the accuracy of the proposed EML and conventional registration methods. CRB is defined as the inverse of the Fisher information matrix ($\boldsymbol{FIM}$) [23], which is the second-order derivative of the expectation of the log likelihood function.

The CRB of the EML registration algorithm is defined as

$$CRB[\boldsymbol{\eta}, \boldsymbol{\xi}(k)] = \boldsymbol{FIM}^{-1} \tag{31}$$

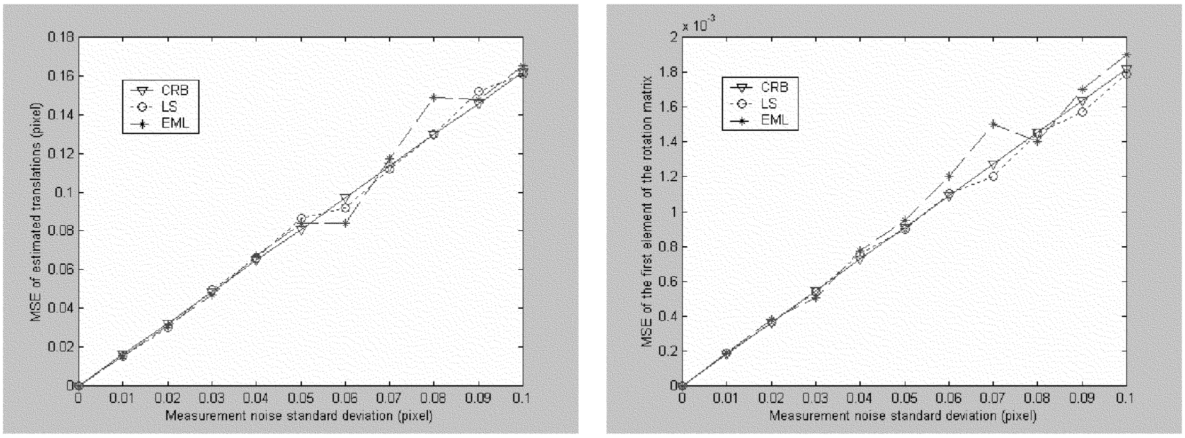

(a) (b)

Fig. 10. Comparison of the CRBs and MSEs of the estimated translations and affine matrix obtained by the EML image registration method and the conventional CP-based LS method. The MSE is plotted versus the CP measurement noise deviation in the subpixel level for the images in Fig. 7(a) and (c). (a)Translation MSE. (b) MSE for the affine matrix. $N_1 = 100$, $N_2 = 0$, and δ_1 changes from 0.0 to 0.10 subpixel. $CRB[\boldsymbol{\eta}] = CRB_1[\boldsymbol{\eta}]$.

where the $\boldsymbol{FIM}$ is given by

$$\boldsymbol{FIM} = \begin{bmatrix} \boldsymbol{F}[\boldsymbol{\eta}] & \boldsymbol{F}[\boldsymbol{\eta}, \boldsymbol{\xi}(k)] \\ \boldsymbol{F}[\boldsymbol{\xi}(k), \boldsymbol{\eta}] & \boldsymbol{F}[\boldsymbol{\xi}(k)] \end{bmatrix}. \tag{32}$$

The elements of the above $\boldsymbol{FIM}$ can be derived as

$$\begin{aligned}
\boldsymbol{F}[\boldsymbol{\eta}] &= E\left[\frac{\partial^2 \Lambda}{\partial \boldsymbol{\eta} \partial \boldsymbol{\eta}}\right] = \frac{1}{\delta_1^2}\sum_{k=1}^{N_1} \boldsymbol{A}^T(k)\boldsymbol{A}(k) + E\left[\frac{\partial^2 \Lambda_2}{\partial \boldsymbol{\eta} \partial \boldsymbol{\eta}}\right] \\
\boldsymbol{F}[\boldsymbol{\xi}(k)] &= E\left[\frac{\partial^2 \Lambda}{\partial \boldsymbol{\xi}(k) \partial \boldsymbol{\xi}(k)}\right] \\
&= \frac{1}{\delta_1^2} diag[\Re^T\Re, \Re^T\Re, \ldots, \Re^T\Re] \\
\boldsymbol{F}[\boldsymbol{\eta}, \boldsymbol{\xi}(k)] &= E\left[\frac{\partial^2 \Lambda}{\partial \boldsymbol{\eta} \partial \boldsymbol{\xi}(k)}\right] = \frac{1}{\delta_1^2}\boldsymbol{A}(k)^T[\Re, \Re, \ldots, \Re] \\
\boldsymbol{F}[\boldsymbol{\xi}(k), \boldsymbol{\eta}] &= E\left[\frac{\partial^2 \Lambda}{\partial \boldsymbol{\xi}(k) \partial \boldsymbol{\eta}}\right] = \boldsymbol{F}[\boldsymbol{\eta}, \boldsymbol{\xi}(k)]^T
\end{aligned} \tag{33}$$

where

$$\Re = -\begin{pmatrix} 1 & 0 & 1 + r_{11} & r_{21} \\ 0 & 1 & r_{12} & 1 + r_{22} \end{pmatrix}^T. \tag{34}$$

From the block matrix inverse theory [25], we have

$$\begin{aligned}
&CRB[\boldsymbol{\eta}] \\
&= \left\{\boldsymbol{F}[\boldsymbol{\eta}] - \boldsymbol{F}[\boldsymbol{\eta}, \boldsymbol{\xi}(k)]\boldsymbol{F}[\boldsymbol{\xi}(k)]^{-1}\boldsymbol{F}[\boldsymbol{\xi}(k), \boldsymbol{\eta}]\right\}^{-1} \\
&= \left\{\sum_{k=1}^{N_1} \frac{1}{\delta_1^2}\left\{\boldsymbol{A}^T(k)\boldsymbol{A}(k) - \boldsymbol{A}^T(k)\Re\left\{\Re^T\Re\right\}^{-1}\Re^T\boldsymbol{A}(k)\right\}\right. \\
&\quad \left. + E\left(\frac{\partial \Lambda_2}{\partial \boldsymbol{\eta}}\right)^T\left(\frac{\partial \Lambda_2}{\partial \boldsymbol{\eta}}\right)\right\}^{-1}
\end{aligned} \tag{35}$$

where $\boldsymbol{P}^{\perp} = \boldsymbol{I} - \boldsymbol{P}$, and $\boldsymbol{P} = \Re\left\{\Re^T\Re\right\}^{-1}\Re^T$. $E\left(\partial\Lambda_2/\partial\boldsymbol{\eta}\right)^T\left(\partial\Lambda_2/\partial\boldsymbol{\eta}\right)$ is given in the Appendix.

Suppose that $CRB_1[\boldsymbol{\eta}]$ is the CRB of the CP-based EML registration algorithm. $CRB_1[\boldsymbol{\eta}]$ can be derived from (38) by letting $E\left(\partial\Lambda_2/\partial\boldsymbol{\eta}\right)^T\left(\partial\Lambda_2/\partial\boldsymbol{\eta}\right) = \boldsymbol{0}$

$$\begin{aligned}
&CRB_1[\boldsymbol{\eta}] = \\
&\left\{\sum_{k=1}^{N_1} \frac{1}{\delta_1^2}\left\{\boldsymbol{A}^T(k)\boldsymbol{A}(k) - \boldsymbol{A}^T(k)\Re\left\{\Re^T\Re\right\}^{-1}\Re^T\boldsymbol{A}(k)\right\}\right\}^{-1}.
\end{aligned} \tag{36}$$

Let $CRB_2[\boldsymbol{\eta}]$ denote the CRB of the conventional intensity-based ML image registration method. Suppose that the number N_1 of CPs is zero in (37), $CRB_2[\boldsymbol{\eta}]$ becomes

$$CRB_2[\boldsymbol{\eta}] = \left\{E\left(\frac{\partial \Lambda_2}{\partial \boldsymbol{\eta}}\right)^T\left(\frac{\partial \Lambda_2}{\partial \boldsymbol{\eta}}\right)\right\}^{-1}. \tag{37}$$

V. Performance Evaluation

In this section, we evaluate the registration performances of the proposed EML and conventional CP-based LS method, and compare them with the corresponding CRBs. We consider the EML image registration algorithm for the following three categories: 1) $N_1 \neq 0$ and $N_2 \neq 0$ (using both CP and intensity); 2) $N_1 \neq 0$ and $N_2 = 0$ (using CP only); 3) $N_1 = 0$ and $N_2 \neq 0$ (using intensity only).

Two cases are investigated here. In the first case, CPs are uniformly distributed in the images. In the second case, CPs have a special distribution. To compare the registration accuracy, distorted images are generated using some known affine transformations. Each test is repeated P times, and we set $P = 100$ in the experiments. In each test, the affine transformation parameters are fixed while the CPs and noisy images are reproduced using the same affine transform and noise variances. The MSE is defined as the average of these 100 trials. The MSE of the x-axis translation is defined as $\sqrt{(1/P)\sum_{p=1}^{P}\left(\hat{t}x(p) - tx\right)^2}$ where $\hat{t}x(p)$ and tx denote the estimate at the pth trial and the

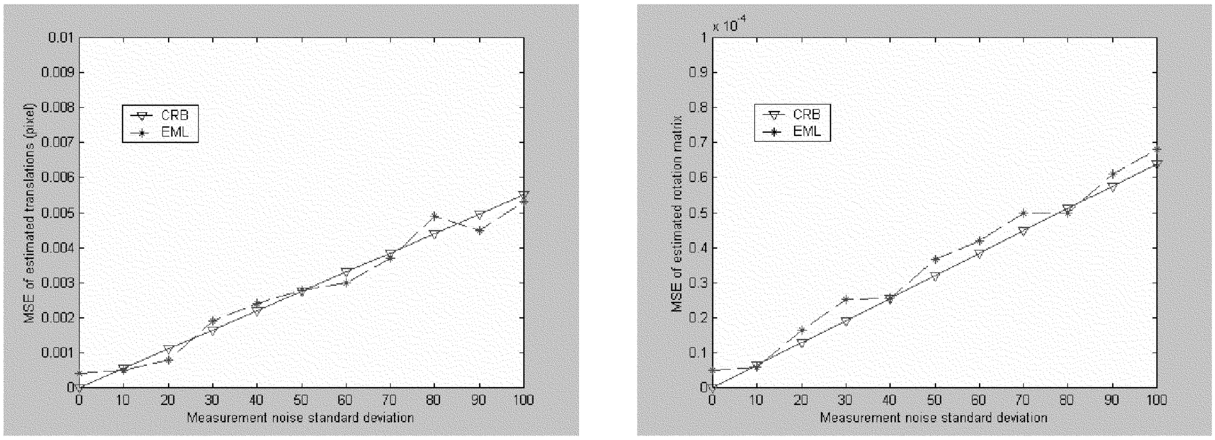

(a) (b)

Fig. 11. Comparison of the CRBs and MSEs of the estimated translations and affine matrix obtained by the intensity-based EML image registration method. The MSE is plotted versus the intensity measurement noise deviation for the image in Fig. 7(a) and (b). (a) Translation MSE. (b) MSE for the affine matrix. $N_1 = 0$, $N_2 = 10\,000$, and δ_2 changes from 0 to 100. $CRB[\boldsymbol{\eta}] = CRB_2[\boldsymbol{\eta}]$.

true x-axis translation, respectively. The MSEs of the y-axis translation and affine matrix elements are defined in a similar fashion. In our study, we only plot the component that has a larger MSE. More precisely, if the MSE of x-axis translation estimate is larger, the estimate of x-axis translation will be depicted for illustration. Similarly, for the affine matrix, the element estimate with the largest MSE among the four elements is chosen for plotting.

A. CPs With Uniform Distribution

In this example, the original and two distorted remote-sensing images are shown in Fig. 2(a)–(c), respectively. In Fig. 2, the maximum gray level is 512. One noisy distorted image with the intensity variance $\delta_2 = 100$ is shown in Fig. 2(c). The size of the images is 128×128. Fig. 3 shows the MSE of the EML algorithm for aligning Fig. 2(a) and (b), and three CRBs: $CRB[\boldsymbol{\eta}]$, $CRB_1[\boldsymbol{\eta}]$, and $CRB_2[\boldsymbol{\eta}]$. The CP measurement noise variance δ_1 changes from 0.01 to 0.1 subpixel. The intensity measurement noise variance δ_2 changes from 10 to 100. When the CP variance is $\delta_1 = 0.01$, the corresponding intensity variance is $\delta_1 = 10$. $N_1 = 200$, $N_2 = 2500$. The CRB of the CP and intensity-based EML approach is lower than both $CRB_1[\boldsymbol{\eta}]$ and $CRB_2[\boldsymbol{\eta}]$. The performance of the EML approach is close to its CRB for all noise levels. Because of limited Monte Carlo trials and computer computation accuracy, the MSE is a little lower than CRB for some samples.

When the intensity information is unavailable, the registration performances of the conventional LS method and the proposed EML method are plotted in Figs. 4 and 5 versus different CP measurement noise levels. If $N_2 = 0$, $CRB[\boldsymbol{\eta}] = CRB_1[\boldsymbol{\eta}]$, and $CRB_2[\boldsymbol{\eta}]$ is unavailable because the intensity-based image registration approach cannot be applied in this case. In Fig. 4, the number of CPs is 100, and the CP measurement noise is in the pixel level. The EML method significantly outperforms the conventional method when the noise level is high. The performance of the proposed EML image registration method is close to the CRBs for all noise levels. However, when the CP measurement noise variance is larger than three pixels, the performance of the CP-based LS method is far worse than the CRBs. For example, the CRB of the translation estimate in Fig. 4(a) is 3.7 pixels when the CP variance is ten pixels. However, the MSE is about 7.4 pixels. The same conclusion is drawn in [19] for the EML-based radar registration problem. Fig. 5 plots the CRBs and MSEs of the EML and conventional CP-based LS methods when the CP measurement noise is in the subpixel level. The performances of both LS and EML methods are close to the CRBs in this case. Both methods obtain registration within subpixel accuracy.

We also consider the situation when there is no CP available. When the number of CPs $N_1 = 0$, $N_2 = 10\,000$, $CRB[\boldsymbol{\eta}] = CRB_2[\boldsymbol{\eta}]$, and $CRB_1[\boldsymbol{\eta}]$ is unavailable because the CP-based image registration approach cannot be applied here. Most of the two images in Fig. 2(a) and (c) are overlapped. Variations of the CRBs and MSEs of the EML approach versus the intensity measurement noise are shown in Fig. 6. When the intensity measurement noise variance δ_2 changes from 0 to 100, the MSEs of estimated translations are below 0.010 subpixel, and the MSEs of estimated affine matrix are below 0.0001. The registration accuracy is high even if the intensity measurement noise is relatively large.

B. CPs With Special Distribution

In many applications, CPs cannot be selected uniformly in the image. For example, CPs must be selected along the coastlines in some ocean remote-sensing images. In the second example, we consider ocean remote-sensing images as shown in Fig. 7. When aligning Fig. 7(a) and (b), both CP and intensity information can be used for registration. However, when aligning Fig. 7(a) with Fig. 7(c), only CPs can be used for registration because the intensity difference between these two images is too large to be suitable for registration. The size of the images is 118×110. Because the number of pixels along the coastline is limited, only 100 CPs are selected.

Fig. 8 evaluates the performance of the proposed EML algorithm for registering Fig. 7(a) and (b) when both CPs and intensity are available. The three CRBs are also depicted for comparison. The parameters are set as $N_1 = 100$, $N_2 = 10\,000$, the CP measurement noise variance δ_1 varies from 0.01 to 0.1 subpixel, and the intensity measurement noise variance δ_2 changes from 10 to 100. The performance of the EML method is close to the CRB which is much lower than $CRB_1[\boldsymbol{\eta}]$, but only a little lower than $CRB_2[\boldsymbol{\eta}]$.

Figs. 9 and 10 evaluate the performance of the proposed EML algorithm for registering Fig. 7(a) and (c) when only CPs are available. Fig. 9 shows the results for the CP measurement noise in the pixel level. When δ_1 is larger than 1 pixel, the estimates of translations and affine matrix by the conventional LS method are far from the CRB. But the performance of the proposed EML method can stay close to the CRB for all noise levels. In Fig. 10, the CP measurement noise is decreased to the subpixel level. The performances of both methods are close to the CRB. When δ_1 is of 0.1 subpixel, the MSEs of estimated translations for coastline-located and uniformly distributed CPs are about 0.16 and 0.04, respectively. Apparently, the registration accuracy based on uniformly distributed CPs is much higher than that of the coastline-located CPs.

Next, we consider the situation that only intensity is used for registration of Fig. 7(a) and (b). We plot the CRB and MSE of the EML image registration method versus the intensity measurement noise in Fig. 11. When the intensity measurement noise variance δ_2 changes from 0 to 50 and $N_2 = 10\,000$, the MSEs of estimated translations are smaller than 0.01 subpixel, and the MSEs of estimated affine matrix are below 0.0001. The accuracy of the proposed registration method is also high for ocean remote-sensing images.

VI. Conclusion

In this paper, we proposed a unified ML model based on both CP and intensity for image registration. An EML method was developed to estimate the registration parameters and CP coordinates in a recursive fashion. The CRBs of the EML and conventional CP and intensity-based image registrations were also derived. The performances of the conventional CP-based LS and the EML image registration methods were evaluated in different situations, and the performances were compared with the CRBs. Through our investigation, we can draw the following conclusions.

The EML approach has a wider application than the conventional CP and intensity-based methods. When both CPs and intensity are available, the accuracy of the proposed EML registration method is higher than both CP and intensity-based approaches. The EML image registration method can also be used to align images when either intensity or CPs are not available. When the CP measurement noise is relatively high, the performance of the proposed EML method that uses only CPs is still close to the CRB while the conventional LS method is far worse than the CRB.

The CRB of the translations and affine matrix elements is not sensitive to the intensity measurement noise variance when most of the two images to be aligned are overlapped. Even if the intensity measurement noise is strong, the accuracy of the proposed EML image registration method using intensity is still high. However, the CRB of the CP-based approaches is more sensitive to the CP measurement noise. When the CP measurement noise variance is in the pixel level, the accuracy of the CP-based registration method is much lower than the intensity-based approaches.

The distributions of the CPs have great effect on the registration accuracy of the CP-based EML and LS registration methods. The registration accuracy will be much higher when CPs are uniformly distributed in the images.

Appendix
Derivation of $E(\partial\Lambda_2/\partial\boldsymbol{\eta})^T(\partial\Lambda_2/\partial\boldsymbol{\eta})$ in (35) and (37)

$E(\partial\Lambda_2/\partial)^T(\partial\Lambda_2/\partial)$ can be derived from (24). The derivatives of Λ_2 with respect to the registration parameter $\boldsymbol{\eta}$ must first be obtained. That is

$$\begin{aligned}\frac{\partial\Lambda_2}{\partial r_{11}} &= \frac{\partial\Lambda_2}{\partial u_1(i)}\frac{\partial u_1(i)}{\partial r_{11}} = \frac{1}{\delta_2^2}\sum_{(i,j)\in\Omega}^{N_2} n_{ij}\frac{\partial f_A(\boldsymbol{u}_1(i,j))}{\partial u_1(i)}u_0(i)\\ \frac{\partial\Lambda_2}{\partial r_{12}} &= \frac{1}{\delta_2^2}\sum_{(i,j)\in\Omega}^{N_2} n_{ij}\frac{\partial f_A(\boldsymbol{u}_1(i,j))}{\partial u_1(i)}v_0(j)\\ \frac{\partial\Lambda_2}{\partial r_{21}} &= \frac{1}{\delta_2^2}\sum_{(i,j)\in\Omega}^{N_2} n_{ij}\frac{\partial f_A(\boldsymbol{u}_1(i,j))}{\partial v_1(j)}u_0(i)\\ \frac{\partial\Lambda_2}{\partial r_{22}} &= \frac{1}{\delta_2^2}\sum_{(i,j)\in\Omega}^{N_2} n_{ij}\frac{\partial f_A(\boldsymbol{u}_1(i,j))}{\partial v_1(j)}v_0(j)\\ \frac{\partial\Lambda_2}{\partial tx} &= \frac{1}{\delta_2^2}\sum_{(i,j)\in\Omega}^{N_2} n_{ij}\frac{\partial f_A(\boldsymbol{u}_1(i,j))}{\partial u_1(i)}\\ \frac{\partial\Lambda_2}{\partial ty} &= \frac{1}{\delta_2^2}\sum_{(i,j)\in\Omega}^{N_2} n_{ij}\frac{\partial f_A(\boldsymbol{u}_1(i,j))}{\partial v_1(j)}.\end{aligned} \tag{38}$$

The elements of $E(\partial\Lambda_2/\partial\boldsymbol{\eta})^T(\partial\Lambda_2/\partial\boldsymbol{\eta})$ are expressed as

$$\begin{aligned}E\left[\frac{\partial\Lambda_2}{\partial r_{11}}\frac{\partial\Lambda_2}{\partial r_{11}}\right] &= \frac{1}{\delta_2^2}\left(\sum_{(i,j)\in\Omega}^{N_2}(f_1u_0(i))^2\right)\\ E\left[\frac{\partial\Lambda_2}{\partial r_{11}}\frac{\partial\Lambda_2}{\partial r_{12}}\right] &= \frac{1}{\delta_2^2}\left(\sum_{(i,j)\in\Omega}^{N_2}f_1^2u_0(i)v_0(j)\right)\\ E\left[\frac{\partial\Lambda_2}{\partial r_{11}}\frac{\partial\Lambda_2}{\partial r_{21}}\right] &= \frac{1}{\delta_2^2}\left(\sum_{(i,j)\in\Omega}^{N_2}f_1f_2u_0^2(i)\right)\\ E\left[\frac{\partial\Lambda_2}{\partial r_{11}}\frac{\partial\Lambda_2}{\partial r_{22}}\right] &= \frac{1}{\delta_2^2}\left(\sum_{(i,j)\in\Omega}^{N_2}f_1f_2u_0(i)v_0(j)\right)\\ E\left[\frac{\partial\Lambda_2}{\partial r_{11}}\frac{\partial\Lambda_2}{\partial tx}\right] &= \frac{1}{\delta_2^2}\left(\sum_{(i,j)\in\Omega}^{N_2}f_1^2u_0(i)\right)\\ E\left[\frac{\partial\Lambda_2}{\partial r_{11}}\frac{\partial\Lambda_2}{\partial ty}\right] &= \frac{1}{\delta_2^2}\left(\sum_{(i,j)\in\Omega}^{N_2}f_1f_2u_0(i)\right)\end{aligned}$$

$$E\left[\frac{\partial\Lambda_2}{\partial r_{12}}\frac{\partial\Lambda_2}{\partial r_{12}}\right] = \frac{1}{\delta_2^2}\left(\sum_{(i,j)\in\Omega}^{N_2} f_1^2 v_0^2(j)\right)$$
$$E\left[\frac{\partial\Lambda_2}{\partial r_{12}}\frac{\partial\Lambda_2}{\partial r_{21}}\right] = \frac{1}{\delta_2^2}\left(\sum_{(i,j)\in\Omega}^{N_2} f_1 f_2 u_0(i) v_0(j)\right)$$
$$E\left[\frac{\partial\Lambda_2}{\partial r_{12}}\frac{\partial\Lambda_2}{\partial r_{22}}\right] = \frac{1}{\delta_2^2}\left(\sum_{(i,j)\in\Omega}^{N_2} f_1 f_2 v_0^2(j)\right)$$
$$E\left[\frac{\partial\Lambda_2}{\partial r_{12}}\frac{\partial\Lambda_2}{\partial tx}\right] = \frac{1}{\delta_2^2}\left(\sum_{(i,j)\in\Omega}^{N_2} f_1^2 v_0(j)\right)$$
$$E\left[\frac{\partial\Lambda_2}{\partial r_{12}}\frac{\partial\Lambda_2}{\partial ty}\right] = \frac{1}{\delta_2^2}\left(\sum_{(i,j)\in\Omega}^{N_2} f_1 f_2 v_0(j)\right)$$
$$E\left[\frac{\partial\Lambda_2}{\partial r_{21}}\frac{\partial\Lambda_2}{\partial r_{21}}\right] = \frac{1}{\delta_2^2}\left(\sum_{(i,j)\in\Omega}^{N_2} (f_2 u_0(i))^2\right)$$
$$E\left[\frac{\partial\Lambda_2}{\partial r_{21}}\frac{\partial\Lambda_2}{\partial r_{22}}\right] = \frac{1}{\delta_2^2}\left(\sum_{(i,j)\in\Omega}^{N_2} f_2^2 u_0(i) v_0(j)\right)$$
$$E\left[\frac{\partial\Lambda_2}{\partial r_{21}}\frac{\partial\Lambda_2}{\partial tx}\right] = \frac{1}{\delta_2^2}\left(\sum_{(i,j)\in\Omega}^{N_2} f_1 f_2 u_0(i)\right)$$
$$E\left[\frac{\partial\Lambda_2}{\partial r_{21}}\frac{\partial\Lambda_2}{\partial ty}\right] = \frac{1}{\delta_2^2}\left(\sum_{(i,j)\in\Omega}^{N_2} f_2^2 u_0(i)\right)$$
$$E\left[\frac{\partial\Lambda_2}{\partial r_{22}}\frac{\partial\Lambda_2}{\partial r_{22}}\right] = \frac{1}{\delta_2^2}\left(\sum_{(i,j)\in\Omega}^{N_2} (f_2 v_0(j))^2\right)$$
$$E\left[\frac{\partial\Lambda_2}{\partial r_{22}}\frac{\partial\Lambda_2}{\partial tx}\right] = \frac{1}{\delta_2^2}\left(\sum_{(i,j)\in\Omega}^{N_2} f_1 f_2 v_0(j)\right)$$
$$E\left[\frac{\partial\Lambda_2}{\partial r_{22}}\frac{\partial\Lambda_2}{\partial ty}\right] = \frac{1}{\delta_2^2}\left(\sum_{(i,j)\in\Omega}^{N_2} f_2^2 v_0(j)\right)$$
$$E\left[\frac{\partial\Lambda_2}{\partial tx}\frac{\partial\Lambda_2}{\partial tx}\right] = \frac{1}{\delta_2^2}\left(\sum_{(i,j)\in\Omega}^{N_2} f_1^2\right)$$
$$E\left[\frac{\partial\Lambda_2}{\partial tx}\frac{\partial\Lambda_2}{\partial ty}\right] = \frac{1}{\delta_2^2}\left(\sum_{(i,j)\in\Omega}^{N_2} f_1 f_2\right)$$
$$E\left[\frac{\partial\Lambda_2}{\partial ty}\frac{\partial\Lambda_2}{\partial ty}\right] = \frac{1}{\delta_2^2}\left(\sum_{(i,j)\in\Omega}^{N_2} f_2^2\right) \qquad (39)$$

where $f_1 = \partial f_A(\boldsymbol{u}_1(i,j))/\partial u_1(i)$, and $f_2 = \partial f_A(\boldsymbol{u}_1(i,j))/\partial v_1(j)$, f_1 and f_2 are computed by using the cubic interpolation method defined in (29). Other elements of $E(\partial\Lambda_2/\partial\boldsymbol{\eta})^T(\partial\Lambda_2/\partial\boldsymbol{\eta})$ are given by

$$E\left[\frac{\partial\Lambda_2}{\partial\eta_i}\frac{\partial\Lambda_2}{\partial\eta_j}\right] = E\left[\frac{\partial\Lambda_2}{\partial\eta_j}\frac{\partial\Lambda_2}{\partial\eta_i}\right]. \qquad (40)$$

References

[1] L. G. Brown, "A survey of image registration techniques," *ACM Comput. Surveys*, vol. 24, no. 4, pp. 325–376, Dec. 1992.

[2] R. A. Schowengerdt, *Remote Sensing Models for Image Processing*. San Diego, CA: Academic, 1997.

[3] R. R. Brooks and S. S. Iyengar, *Multi-Sensor Fusion: Fundamentals and Applications with Software*. Upper Saddle River, NJ: Prentice-Hall, 1998.

[4] J. B. A. Maintz and M. A. Viergever, "A survey of medical image registration," *Med. Image Anal.*, vol. 2, no. 1, pp. 1–36, Apr. 1998.

[5] Y. Bresler and S. J. Merhav, "Recursive image registration with application to motion estimation," *IEEE Trans. Acoust., Speech, Signal Processing*, vol. ASSP-35, pp. 70–85, Jan. 1987.

[6] J. Townshend, C. Justice, C. Gurney, and J. McManus, "The impact of misregistration on change detection," *IEEE Trans. Geosci. Remote Sensing*, vol. 30, pp. 1054–1060, Nov. 1992.

[7] Z. Yang and F. S. Cohen, "Image registration and object recognition using affine invariants and convex hulls," *IEEE Trans. Image Processing*, vol. 8, pp. 934–946, July 1999.

[8] J. Ton and A. K. Jain, "Registering Landsat images by point matching," *IEEE Trans. Geosci. Remote Sensing*, vol. 27, pp. 642–651, Sept. 1989.

[9] S. Gold, A. Rangarajan, C. Lu, S. Pappu, and E. Mjolsness, "New algorithms for 2D and 3D point matching pose estimation and correspondence," *Pattern Recognit.*, vol. 31, no. 8, pp. 1019–1031, 1998.

[10] Z. Mao, D. Pan, H. Huang, and W. Huang, "Automatic registration of SeaWiFS and AVHRR imagery," *Int. J. Remote Sensing*, vol. 22, no. 9, pp. 1725–1735, June 2001.

[11] K. S. Arun, T. S. Huang, and S. D. Blostein, "Least-squares fitting of two 3-D point sets," *IEEE Trans. Pattern Anal. Machine Intell.*, vol. PAMI-9, pp. 698–700, Sept. 1987.

[12] S. Umeyama, "Least-squares estimation of transformation parameters between two point patterns," *IEEE Trans. Pattern Anal. Machine Intell.*, vol. 13, pp. 376–380, Apr. 1991.

[13] P. A. Van Den Elsen, E. D. Pol, T. S. Sumanaweera, P. F. Her, S. Napel, and J. R. Adler, "Grey value correlation techniques used for automatic matching of CT and MR brain and spine images," in *Proc. SPIE Visualization in Biomedical Computing*, vol. 2357, 1994, pp. 227–237.

[14] P. Thevenaz, U. E. Ruttimann, and M. Unser, "A pyramid approach to subpixel registration based on intensity," *IEEE Trans. Image Processing*, vol. 7, pp. 27–41, Jan. 1998.

[15] M. S. Mort and M. D. Srinath, "Maximum likelihood image registration with subpixel accuracy," in *Proc. SPIE*, vol. 974, San Diego, CA, Aug. 1988, pp. 38–45.

[16] W. L. S. Costa, D. R. Haynor, R. M. Haralick, T. K. Lwellen, and M. M. Graham, "A maximum-likelihood approach to PET emission/attenuation image registration," in *IEEE Nuclear Science Symp. Medical Imaging Conf.*, 1993.

[17] H. J. Johnson and G. E. Christensen, "Consistent landmark and intensity-based image registration," *IEEE Trans. Med. Imag.*, vol. 21, pp. 450–461, May 2002.

[18] P. Hellier and C. Barillot, "Coupling dense and landmark-based approaches for nonrigid registration," *IEEE Trans. Med. Imag.*, vol. 22, pp. 217–227, Feb. 2003.

[19] Y. Zhou, H. Leung, and P. C. Yip, "An exact maximum likelihood registration algorithm for data fusion," *IEEE Trans. Signal Processing*, vol. 45, pp. 1560–1573, June 1997.

[20] F. Rice, B. Cowley, and M. Rice, "Cramer-Rao lower bounds for QAM phases and frequency estimation," *IEEE Trans. Commun.*, vol. 49, pp. 1582–1591, Sept. 2001.

[21] X. Liu and N. D. Sidropoulos, "Cramer-Rao lower bounds for low-rank decomposition of multidimensional arrays," *IEEE Trans. Signal Processing*, vol. 49, pp. 2074–2086, Sept. 2001.

[22] A. Dogandzic and A. Nehorai, "Cramer-Rao bounds for estimating range, velocity, and direction with an active array," *IEEE Trans. Signal Processing*, vol. 49, pp. 1122–1137, June 2001.

[23] T. W. Anderson, *An Introduction of Multivariate Statistical Analysis*. New York: Wiley, 1984.

[24] R. G. Keys, "Cubic convolution interpolation for digital image processing," *IEEE Trans. Acoust., Speech, Signal Processing*, vol. ASSP-29, pp. 1153–1160, Dec. 1981.

[25] G. H. Golub and C. F. Van Loan, *Matrix Computation*. Baltimore, MD: Johns Hopkins Univ. Press, 1990.

Winston Li received the B.S. and M.S. degrees in electrical engineering from the Radio Department, Northwestern Polytechnic University, Fremont, CA, in 1988 and 1991, respectively, and the Ph.D. degree in electrical engineering from the Department of Electrical Engineering, Xidian University, Xi'an, China, in 1995.

From 1995 to 1997, he designed adaptive channel equalization and RAKE receivers for IS95 CDMA as a Postdoctoral Research Fellow in the Radio Department, Southeast University, Nanjing, China. From 1998 to 1999, he developed circuit exchange and image monitoring systems as a Team Leader at Dongfang Electronics Company, Yantai, China. From 2000 to 2001, he was a Technical Manager of the IP/ATM and WCDMA projects with Eastcom Company, Hangzhou, China. Since 2001, he has been a Postdoctoral Research Fellow in Department of Electrical and Computer Engineering, University of Calgary, Calgary, AB, Canada. His main research interests are in 3G and beyond, IP/ATM, smart antenna, vehicle localization and navigation by fusing GPS/INS/radar/camera, and intelligent transportation systems.

Henry Leung (M'90) received the Ph.D. degree in electrical and computer engineering from McMaster University, Hamilton, ON, Canada.

He is currently a Professor with the Department of Electrical and Computer Engineering, University of Calgary, Calgary, ON. He was with the Defence Research Establishment Ottawa, ON, where he was involved in the design of automated systems for air and maritime multisensor surveillance. His research interests include chaos, computational intelligence, data mining, nonlinear signal processing, multimedia, and wireless communications.